pISSN: 2321-9742

Advances in Physical Science Research

The Sapience

Physics and Applications of Metamaterials

Isht Vibhu[1,a], Vishal Singh Chandel[2,b]

[1]Department of Physics, Yuveraj Dutta Postgraduate College, Lakhimpur Kheri-262701, India
[2]Department of Physics, Integral University, Kursi Road, Lucknow, 226026, India

Emails: [a]ishtvibhu@gmail.com, [b]chandel.integral@gmail.com

Abstract

Metamaterials are artificially structured composite materials that show negative effective refractive index over certain frequency bands. This has led to novel control over electromagnetic wave propagation. This paper extends a preliminary lecture presented at a Conference (Emerging Trends in Non-Conventional Energy Recourses(ETNCER-16), 2016) by comprehensively examining the fundamental physics behind metamaterials and also the history of the development. A brief summary of exotic properties of metamaterials is also presented. The underlying mechanisms of negative permittivity and permeability are explained. Various remarkable phenomena such as perfect lensing, electromagnetic cloaking, and reversed electromagnetic effects are also discussed here in a pedagogically relevant manner. Their emerging applications are also briefly reviewed here, with particular emphasis on their applications in energy harvesting, wireless power transmission, cloaking and thermophotovoltaic energy conversion.

1 Introduction

Propagation of light through material has been developed using the Maxwell's equations of electromagnetism and established that the refractive index of the material is a result of the properties of the material, namely, permittivity and permeability. Permittivity and permeability were either a positive real number or complex number in a lossy medium. Veselago [1] had first investigated a mathematically consistent case of materials which may have simultaneous negative effective permittivity ϵ and negative effective permeability μ. He analytically showed that such materials, now known as metamaterials, have unusual reversed electromagnetic-wave propagation phenomena.

Smith et. al. have reported successful fabricationo of such materials in the early 2000s [3, 4]. Since then, these artificially structured composite materials,i.e., electromagnetic metamaterials, have been explored for their exotic properties and potential engineering applications. Though the defining characteristic of metamaterials is their exhibition of frequency bands where the effective refractive index becomes negative, arising from simultaneously negative electric permittivity ($\epsilon < 0$) and magnetic permeability ($\mu < 0$) [1, 5], they possess the remarkable ability to manipulate electromagnetic waves in hitherto unexpected ways and extraordinary electromagnetic properties.In contrast to traditional materials, which exhibit characteristics based primarily on their chemical composition , metamaterials acquire their properties from its structure which is artificially engineered at dimensions significantly smaller than the wavelengths of the electromagnetic radiation they engage with. This fabrication has helped realize the properties which were initially proposed only theoretically and has led to the identification of completely novel physical properties. These properties have made the metamaterials important for photonics, telecommunications, and energy applications and the scientific community has witnessed an explosion of interest in metamaterial applications for energy-related technologies . Whether it is the purpose of harvesting ambient RF radiation to enhancing solar cell efficiency, or development of next-generation thermophotovoltaic converters is needed, metamaterials promise to play a crucial role in addressing global energy challenges. This review overviews metamaterial physics, exotic electromagnetic phenomena, and their emerging applications.

2 Fundamental Concepts and Their Experimental Realisation

This section summarises the theoretical foundation and the standardized terminology essential for the study of electromagnetic metamaterials. Electromagnetic waves interact with the medium and the nature of this interaction determines the nature of wave propagation. This interaction is established using the framework of Maxwell's equations, with the properties of the medium coming into play through their constitutive parameters, ϵ and μ.

2.1 Summary of Electromagnetism of Wave Propagation in Material Medium

The propagation of electromagnetic waves in a linear, isotropic, and homogeneous medium is governed by Maxwell's equations and has been thoroughly discussed in the graduation level standard textbooks. For the sake of convenience, a summary of it is being produced

here. As is known, the fields of Maxwell's equations, viz., electric field $\mathbf{E}$, magnetic field $\mathbf{H}$, electric displacement $\mathbf{D}$, and magnetic induction $\mathbf{B}$ are connected through the constitutive relations:

$$\mathbf{D} = \epsilon\mathbf{E} = \epsilon_0\epsilon_r\mathbf{E} \tag{1}$$

$$\mathbf{B} = \mu\mathbf{H} = \mu_0\mu_r\mathbf{H} \tag{2}$$

where $\epsilon = \epsilon_0\epsilon_r$ is the absolute permittivity (ϵ_0 is the vacuum permittivity, ϵ_r is the relative permittivity), and $\mu = \mu_0\mu_r$ is the absolute permeability (μ_0 is the vacuum permeability, μ_r is the relative permeability). For source-free regions, Maxwell's curl equations in the time domain are:

$$\nabla \times \mathbf{E} = -\frac{\partial \mathbf{B}}{\partial t} = -\mu\frac{\partial \mathbf{H}}{\partial t} \tag{3}$$

$$\nabla \times \mathbf{H} = \frac{\partial \mathbf{D}}{\partial t} = \epsilon\frac{\partial \mathbf{E}}{\partial t} \tag{4}$$

Assuming harmonic time dependence $e^{j\omega t}$ for monochromatic waves, where ω is the angular frequency, the time derivative transforms as $\frac{\partial}{\partial t} \rightarrow j\omega$. Maxwell's equations in the frequency domain become:

$$\nabla \times \mathbf{E} = -j\omega\mu\mathbf{H} \tag{5}$$

$$\nabla \times \mathbf{H} = j\omega\epsilon\mathbf{E} \tag{6}$$

For a plane wave propagating with wave vector $\mathbf{k}$, the spatial dependence of the fields is:

$$\mathbf{E}(\mathbf{r}, t) = \mathbf{E}_0 e^{j(\omega t - \mathbf{k}\cdot\mathbf{r})} \tag{7}$$

$$\mathbf{H}(\mathbf{r}, t) = \mathbf{H}_0 e^{j(\omega t - \mathbf{k}\cdot\mathbf{r})} \tag{8}$$

where $\mathbf{E}_0$ and $\mathbf{H}_0$ are the complex field amplitudes, and $\mathbf{r}$ is the position vector.

The curl operator acting on a plane wave field yields:

$$\begin{aligned}\nabla \times \mathbf{E} &= \left(\hat{i}\frac{\partial}{\partial x} + \hat{j}\frac{\partial}{\partial y} + \hat{k}\frac{\partial}{\partial z}\right) \times \mathbf{E}_0 e^{j(\omega t - \mathbf{k}\cdot\mathbf{r})} \\ &= \mathbf{E}_0 e^{j(\omega t - \mathbf{k}\cdot\mathbf{r})} \times (-j\mathbf{k}) \\ &= -j\mathbf{k} \times \mathbf{E}\end{aligned} \tag{9}$$

Applying the same procedure to equation (6):

$$\nabla \times \mathbf{H} = -j\mathbf{k} \times \mathbf{H} \tag{10}$$

Substituting these plane wave expressions into equations (5) and (6), we obtain:

$$\mathbf{k} \times \mathbf{E} = \omega\mu\mathbf{H} \tag{11}$$

$$\mathbf{k} \times \mathbf{H} = -\omega\epsilon\mathbf{E} \tag{12}$$

Taking the cross product of equation (11) with $\mathbf{k}$:

$$\begin{aligned} \mathbf{k} \times (\mathbf{k} \times \mathbf{E}) &= \omega\mu(\mathbf{k} \times \mathbf{H}) \\ \mathbf{k}(\mathbf{k} \cdot \mathbf{E}) - \mathbf{E}(\mathbf{k} \cdot \mathbf{k}) &= \omega\mu(-\omega\epsilon\mathbf{E}) \quad \text{(using vector identity)} \\ \mathbf{k}(\mathbf{k} \cdot \mathbf{E}) - k^2\mathbf{E} &= -\omega^2\epsilon\mu\mathbf{E} \end{aligned} \tag{13}$$

For a transverse electromagnetic (TEM) wave, $\mathbf{k} \perp \mathbf{E}$, so $\mathbf{k} \cdot \mathbf{E} = 0$. This yields the fundamental dispersion relation:

$$k^2 = \omega^2\epsilon\mu \tag{14}$$

Similarly, one can show that $\mathbf{k}\cdot\mathbf{H} = 0$, confirming that both $\mathbf{E}$ and $\mathbf{H}$ are perpendicular to the propagation direction $\mathbf{k}$.

The magnitude of the wave vector is:

$$k = \omega\sqrt{\epsilon\mu} \tag{15}$$

The refractive index n is defined as the ratio of the speed of light in vacuum c to the phase velocity in the medium $v_p = \omega/k$:

$$n = \frac{c}{v_p} = \frac{ck}{\omega} = c\sqrt{\epsilon\mu} = \sqrt{\epsilon_r\mu_r} \tag{16}$$

where we used $c = 1/\sqrt{\epsilon_0\mu_0}$.

2.2 Wave Propagation in Conventional and Single-Negative Media

Before Veselago's seminal work in 1964, physicists understood electromagnetic wave propagation in three distinct regimes based on the signs of permittivity ϵ and permeability μ. This section presents the pre-1964 understanding that formed the foundation for Veselago's revolutionary insights.

2.2.1 Double-Positive (DPS) Media: Conventional Dielectrics

In ordinary dielectric materials where both $\epsilon > 0$ and $\mu > 0$, the dispersion relation $k^2 = \omega^2\epsilon\mu$ yields a real wave vector:

$$k = \omega\sqrt{\epsilon\mu} > 0 \tag{17}$$

Electromagnetic waves propagate without exponential decay. The wave impedance is:

$$Z = \sqrt{\frac{\mu}{\epsilon}} > 0 \tag{18}$$

The time-averaged Poynting vector $\langle \mathbf{S} \rangle = \frac{1}{2}\mathrm{Re}[\mathbf{E} \times \mathbf{H}^*]$ and wave vector $\mathbf{k}$ are parallel, indicating that phase velocity and energy flow are in the same direction:

$$\langle \mathbf{S} \rangle = \frac{|E_0|^2}{2\omega\mu} k\hat{z} \quad \text{with} \quad k > 0, \mu > 0 \quad \Rightarrow \quad \langle \mathbf{S} \rangle \parallel \mathbf{k} \tag{19}$$

This regime represents all the conventional transparent materials like air, glass, water, and most of the dielectrics. In this regime, the refractive index $n = \sqrt{\epsilon_r\mu_r}$ is positive, and Snell's law describes refraction at interfaces in the familiar manner.

In DPS media, the electric field $\mathbf{E}$, magnetic field $\mathbf{H}$, and wave vector $\mathbf{k}$ form a right-handed orthogonal triplet system; this is illustrated in Figure 1. The right-handedness implies when fingers of right hand curl from $\mathbf{E}$ toward $\mathbf{H}$, the thumb points along $\mathbf{k}$ (and $\mathbf{S}$). This fundamental geometric relationship ensures that phase propagation and energy flow proceed in the same direction; this is the conventional wave behavior.

2.2.2 Epsilon-Negative (ENG) Media: Metals and Plasmas

The electromagnetic behavior of metals at optical frequencies was understood by the early 20th century through the Drude model (1900) and developments in plasma physics during the 1920s-1940s. By the 1960s, negative permittivity in conducting materials was textbook knowledge. The Drude-Lorentz dispersion model for the permittivity of a conductor or plasma is [6]:

$$\epsilon(\omega) = \epsilon_0 \left(1 - \frac{\omega_p^2}{\omega^2 + j\gamma\omega}\right) \tag{20}$$

where $\omega_p = \sqrt{n_e e^2/(\epsilon_0 m_e)}$ is the plasma frequency determined by the free electron density n_e, electron charge e, electron mass m_e, and γ is the collision frequency representing losses.

For frequencies below the plasma frequency ($\omega < \omega_p$) and neglecting losses ($\gamma \to 0$):

$$\epsilon(\omega) = \epsilon_0 \left(1 - \frac{\omega_p^2}{\omega^2}\right) < 0 \quad \text{while} \quad \mu \approx \mu_0 > 0 \tag{21}$$

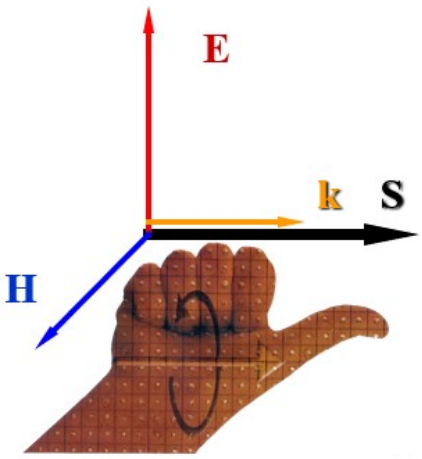

Figure 1: Right-handed electromagnetic triplet in conventional DPS media. The electric field **E** (red), magnetic field **H** (blue), and wave vector **k** constitute a right-handed orthogonal system. The Poynting vector **S** (representing energy flow) is parallel to **k** (phase velocity direction), demonstrating that energy and phase propagate together in the same direction. The right-hand rule visualization shows how these vectors are oriented: fingers curling from **E** to **H** point the thumb along **k**.

For these frequencies,we have with $\epsilon < 0$ and $\mu > 0$ and the wave propagation characteristics are determined by the dispersion relation which becomes:

$$k^2 = \omega^2 \epsilon \mu = \omega^2(-|\epsilon|)\mu < 0 \tag{22}$$

This yields a purely imaginary wave vector $k = j\alpha$ where $\alpha = \omega\sqrt{|\epsilon|\mu}$ is the attenuation constant. The electromagnetic fields take the form:

$$\mathbf{E}(z,t) = \mathbf{E}_0 e^{-\alpha z} e^{j\omega t} \tag{23}$$

This can be interpreted as a signal with exponentially decaying amplitude. Thus, the electromagnetic waves cannot propagate into the medium; instead, they decay exponentially from the surface with a characteristic skin depth:

$$\delta = \frac{1}{\alpha} = \frac{1}{\omega\sqrt{|\epsilon|\mu}} \tag{24}$$

This exponential decay explains why metals are highly reflective at optical frequencies—electromagnetic energy cannot penetrate beyond a thin surface layer. The incident wave induces surface currents that re-radiate, producing the reflected wave.

There are many real examples of ENG media such as noble metals (Au, Ag, Cu) at visible and UV frequencies: $\omega_p \sim 10^{15}$ rad/s,the Earth's ionosphere for radio waves below ∼10 MHz: $\omega_p \sim 10^7$ rad/s, dense plasmas in controlled fusion reactors and astrophysical environments, and many other. These have found many technological applications, such

as, reflective coatings and mirrors, radio wave propagation and long-distance communication via ionospheric reflection,electromagnetic shielding and many others.

By the 1960s, epsilon-negative behavior was thoroughly understood theoretically and exploited extensively in plasma physics, radio engineering, and optics.

2.2.3 Mu-Negative (MNG) Media: Magnetic Resonators

The negative value of permeability is a result of ferromagnetic resonance (FMR), a phenomenon first reported by Griffiths in 1946 [**?**]. Although the initial discovery focused on anomalous microwave absorption and surface resistance in ferromagnetic metals, modern effective medium theory interprets the phase-lagged response near resonance as a window of negative effective permeability ($\mu_{eff} < 0$). When a ferromagnetic material is subjected to two magnetic fields simultaneously: one is a static magnetic field $\mathbf{H}_0$, and the other is a small oscillating perpendicular field, the magnetization vector $\mathbf{M}$ starts to precess around $\mathbf{H}_0$. This precession occurs at a frequency that depends on both the applied field strength and the material's saturation magnetization M_s. Kittel derived a formula for a spherical sample:

$$\omega_0 = \gamma\mu_0\sqrt{H_0(H_0 + M_s)} \tag{25}$$

where γ is the gyromagnetic ratio.

For frequencies just below resonance, the real part of the permeability attains negative values while the permittivity remains positive. This occurs because the precessional motion lags behind the driving field by approximately 180°. This causes the induced magnetic response to oppose rather than reinforce the applied field. In this single-negative regime ($\epsilon > 0$, $\mu < 0$), the wave vector becomes purely imaginary and electromagnetic waves decay exponentially as evanescent modes.

Common materials exhibiting this behavior include yttrium iron garnet (YIG) spheres, and various magnetized ferrites such as nickel ferrite and manganese ferrite. Despite being well-characterized by the early 1960s, these materials presented severe limitations. The negative permeability occurs only within an extremely narrow bandwidth, typically just a few MHz around resonance. Achieving FMR requires bulky external magnets. Energy dissipation causes significant absorption. Thus, the negative value of permittivity with simultaneous occurance of negative value of permeability at the same frequency was not observed in any material.

2.2.4 The Pre-Veselago Understanding: Three Known Regimes

By the early 1960s, the scientific community recognized three distinct electromagnetic regimes based on the signs of permittivity and permeability. In conventional double-positive (DPS) media where both $\epsilon > 0$ and $\mu > 0$, the wave vector $k = \omega\sqrt{\epsilon\mu}$ is real,

allowing electromagnetic waves to propagate freely with phase velocity and energy flow in the same direction. All ordinary dielectrics fall into this category.

The epsilon-negative (ENG) regime, where $\epsilon < 0$ while $\mu > 0$, was familiar from the behavior of metals below their plasma frequency. In this regime, the wave vector becomes purely imaginary ($k = j\alpha$), and this resulted in producing evanescent waves that decay exponentially without propagating energy. This accounts for the characteristic metallic reflection of electromagnetic radiation.

Similarly, the mu-negative (MNG) regime with $\epsilon > 0$ but $\mu < 0$ had been well-characterized in magnetized ferrites near their ferromagnetic resonance frequencies. Like the ENG case, the imaginary wave vector produces evanescent behavior with strong absorption or reflection. However, this phenomenon was confined to narrow frequency bands around magnetic resonance and required external magnetic fields.

The fourth quadrant of parameter space was characterized by $\epsilon < 0$ and $\mu < 0$ simultaneously and this remained completely unexplored. Several factors contributed to this oversight. No known natural materials exhibited both negativities at the same frequency; metals retain positive permeability while magnetic materials have positive permittivity. Since both the ENG and MNG regimes individually produce evanescent waves, it might have been implicitly assumed that combining the two would yield similar or even stronger attenuation. Without any conceivable means to fabricate materials with simultaneous negative parameters, there was no practical motivation to investigate this hypothetical regime theoretically. Most critically, no one had recognized the fundamental mathematical distinction that $\epsilon\mu = (-|\epsilon|)(-|\mu|) > 0$ in the double-negative case, making it qualitatively different from either single-negative regime.

This conceptual gap persisted until Viktor Veselago's 1964 analysis revealed the revolutionary physics hidden in this unexplored quadrant.

2.3 Veselago's Revolutionary Insight: The Double-Negative Regime (1964)

Viktor Veselago established the theoretical foundations of metamaterials in his seminal 1964 paper, "The Electrodynamics of Substances with Simultaneously Negative Values of ϵ and μ" [1]. Working purely from theoretical considerations—as no such materials were known to exist in nature—Veselago systematically explored the previously neglected fourth quadrant of electromagnetic parameter space.

Veselago recognized that when *both* $\epsilon < 0$ and $\mu < 0$ simultaneously:

$$k^2 = \omega^2\epsilon\mu = \omega^2(-|\epsilon|)(-|\mu|) = \omega^2|\epsilon||\mu| > 0 \tag{26}$$

Unlike ENG and MNG media where $\epsilon\mu < 0$ produces imaginary k (evanescence), in

double-negative (DNG) media $\epsilon\mu > 0$ yields a *real* wave vector (propagation)!

$$k = \pm\omega\sqrt{|\epsilon||\mu|} \quad \text{(real, not imaginary!)} \tag{27}$$

Despite both fundamental electromagnetic parameters being negative, waves can *propagate* rather than decay exponentially. This double-negative regime is found to be fundamentally different from the single-negative regimes.

While k^2 is positive, yielding real solutions, the square of the refractive index $n^2 = \epsilon\mu$ also remains positive in DNG media. However, Veselago demonstrated that the underlying physics of wave propagation is fundamentally altered from conventional materials.

Veselago was the first to systematically classify all four possible combinations of ϵ and μ signs:

Table 1: Veselago's four-quadrant classification of electromagnetic media (1964)

ϵ	μ	$\epsilon\mu$	k	Wave	**Medium behavior**
$+$	$+$	$+$	Real	Propagating	Conventional dielectrics (DPS)
$-$	$+$	$-$	Imaginary	Evanescent	Metals/plasmas (ENG)
$+$	$-$	$-$	Imaginary	Evanescent	Magnetic resonators (MNG)
$-$	$-$	$+$	Real	**Propagating**	**Left-handed media (DNG)**

While the physical phenomena underlying epsilon-negative (metals below plasma frequency) and mu-negative (ferrites near ferromagnetic resonance) regimes were well established before Veselago's 1964 work through extensive experimental and theoretical studies, his fundamental contribution was recognizing that the double-negative regime exhibits qualitatively different physics—propagating waves with reversed electromagnetic properties—rather than the evanescent behavior of single-negative media.

2.3.1 The Refractive Index Ambiguity and Sign Choice

From the dispersion relation $k^2 = \omega^2\epsilon\mu$, when both $\epsilon < 0$ and $\mu < 0$, we obtain:

$$k = \pm\omega\sqrt{|\epsilon||\mu|} \tag{28}$$

The refractive index $n = ck/\omega$ can therefore be either positive or negative. The critical question becomes: *which sign should be chosen?*

Veselago argued that if ϵ and μ are both positive, the vectors $\mathbf{E}$, $\mathbf{H}$, and $\mathbf{k}$ form a right-handed triplet. However, if $\epsilon < 0$ and $\mu < 0$, these same Maxwell equations force the set to become a *left-handed* triplet. The resolution comes from requiring that energy propagates in a physically meaningful direction consistent with causality. For a wave propagating in the $+z$ direction, the Poynting vector (representing energy flux) can be shown to be:

$$\mathbf{S} = \frac{|\mathbf{E}|^2}{\omega\mu}\mathbf{k} \tag{29}$$

When $\mu < 0$ in DNG media, the sign of the Poynting vector relative to $\mathbf{k}$ depends critically on the choice of k:

- **If we choose** $k = +\omega\sqrt{|\epsilon||\mu|}$ (positive root):

  The Poynting vector becomes:

$$\mathbf{S} = \frac{|\mathbf{E}|^2}{\omega\mu}\mathbf{k} = \frac{|\mathbf{E}|^2}{\omega(-|\mu|)}(+\omega\sqrt{|\epsilon||\mu|})\hat{z} \propto -\hat{z} \tag{30}$$

  The Poynting vector points in the $-z$ direction, indicating energy flow *toward* the source rather than away from it. This violates causality: energy would appear at locations that the source has not yet reached, effectively requiring energy to propagate backward in time or to materialize spontaneously in regions where no source exists.

- **If we choose** $k = -\omega\sqrt{|\epsilon||\mu|}$ (negative root):

  The Poynting vector becomes:

$$\mathbf{S} = \frac{|\mathbf{E}|^2}{\omega\mu}\mathbf{k} = \frac{|\mathbf{E}|^2}{\omega(-|\mu|)}(-\omega\sqrt{|\epsilon||\mu|})\hat{z} \propto +\hat{z} \tag{31}$$

  The Poynting vector points in the $+z$ direction, indicating energy flow *away from* the source. This ensures that electromagnetic energy reaches distant points only after propagating outward from the source location, and thus preserves causality.

The fundamental requirement that energy must flow away from its source (not toward it) forces us to select the *negative* root:

$$n = -\sqrt{\epsilon\mu} = -\sqrt{|\epsilon||\mu|} \quad \text{for DNG media} \tag{32}$$

This choice ensures that $\mathbf{k}$ and $\langle\mathbf{S}\rangle$ are *antiparallel*: phase fronts propagate backward (in the $-z$ direction) while energy flows forward (in the $+z$ direction). This represents **backward-wave propagation** in double-negative metamaterials.

Physical interpretation: An observer watching electromagnetic waves in a DNG medium would witness phase fronts moving in the opposite direction to energy transport. The peaks and troughs of the wave pattern move backward, yet electromagnetic energy flows forward. This counterintuitive behavior distinguishes left-handed media from all conventional materials.

2.3.2 Veselago's Dispersion and Energy Density Arguments

Veselago further justified the negative index choice through fundamental energy considerations. In a dispersive medium, the time-averaged electromagnetic energy density is not

simply $\frac{1}{2}(\epsilon|\mathbf{E}|^2 + \mu|\mathbf{H}|^2)$—which would be negative and unphysical for DNG media—but rather:

$$W = \frac{1}{4}\left[\frac{\partial(\omega\epsilon)}{\partial\omega}|\mathbf{E}|^2 + \frac{\partial(\omega\mu)}{\partial\omega}|\mathbf{H}|^2\right] \tag{33}$$

For the energy density to remain positive (a fundamental physical requirement), Veselago proved that ϵ and μ must exhibit frequency dispersion satisfying:

$$\frac{\partial(\omega\epsilon)}{\partial\omega} > 0 \quad \text{and} \quad \frac{\partial(\omega\mu)}{\partial\omega} > 0 \tag{34}$$

DNG behavior can only occur over limited frequency ranges where specific resonance conditions are met. This dispersion requirement, combined with causality constraints via the Kramers-Kronig relations, uniquely determines that the negative refractive index branch must be chosen for double-negative media.

The group velocity, which determines energy transport, is:

$$v_g = \frac{d\omega}{dk} \tag{35}$$

With the proper dispersion relations and the negative sign choice for k, Veselago showed that $v_g > 0$, confirming that energy propagates in the physically correct direction.

2.3.3 The Left-Handed Electromagnetic Triplet

To quantify the handedness of the electromagnetic field configuration, Veselago introduced a parameter p to characterize the "rightness" of the medium:

$$p = \frac{\mathbf{E} \cdot (\mathbf{H} \times \mathbf{k})}{|\mathbf{E} \cdot (\mathbf{H} \times \mathbf{k})|} \tag{36}$$

For conventional right-handed media (DPS), the vectors $\mathbf{E}$, $\mathbf{H}$, and $\mathbf{k}$ form a right-handed triplet, giving $p = +1$. For left-handed media (DNG), these vectors form a left-handed triplet, yielding $p = -1$. This parameter provides a parameter which distinguishes the two classes of materials based on the orientation of their electromagnetic field triplet.

From Maxwell's curl equations:

$$\mathbf{k} \times \mathbf{E} = \omega\mu\mathbf{H} \tag{37}$$

$$\mathbf{k} \times \mathbf{H} = -\omega\epsilon\mathbf{E} \tag{38}$$

In conventional right-handed materials where $\epsilon_r > 0$ and $\mu_r > 0$, the electric field $\mathbf{E}$, magnetic field $\mathbf{H}$, and wave vector $\mathbf{k}$ form a right-handed orthogonal triplet with phase velocity parallel to energy flow. In left-handed materials, these vectors form a left-handed triplet with $\mathbf{k}$ and $\mathbf{S}$ antiparallel. Figure 2 illustrates this left-handed electromagnetic

configuration in DNG media, where the electric field **E** (red), magnetic field **H** (blue), and wave vector **k** (orange) form a left-handed system. Critically, the Poynting vector **S** (black), representing energy flow, points opposite to **k**, demonstrating that energy and phase propagate in opposite directions. The left-hand rule visualization shows how these vectors are oriented: when fingers curl from **E** to **H**, the thumb points along **k**, but energy flows in the opposite direction along **S**.

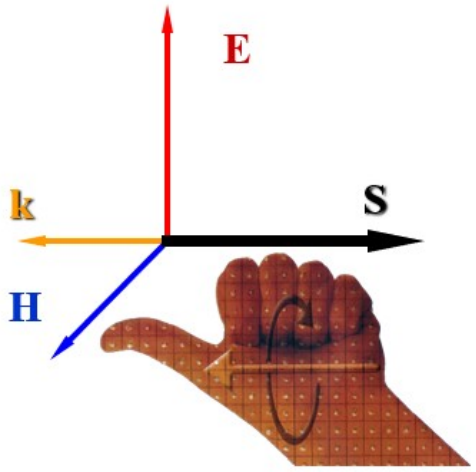

Figure 2: Left-handed electromagnetic triplet in DNG media. The electric field **E** (red), magnetic field **H** (blue), and wave vector **k** (orange) form a left-handed orthogonal system. The Poynting vector **S** (black, representing energy flow) is antiparallel to **k** (phase velocity direction), demonstrating that energy and phase propagate in opposite directions. The left-hand rule visualization shows how these vectors are configured: fingers curling from **E** to **H** point the thumb along **k**, while energy flows opposite to this direction.

2.4 Popular Terms and Their Equivalence

At present, electromagnetic metamaterials are defined as the artificially structured composite materials which have been specifically engineered to have both permeability and permittivity negative. These materials have been found to exhibit electromagnetic properties which have not been found in nature. The scientific community uses several equivalent terms to describe such metamaterials. "Negative Index Materials" (NIM) emphasizes the negative refractive index, while "Double Negative Materials" (DNG or DNM) directly references the sign of the constitutive parameters. "Left-Handed Materials" (LHM) describes the geometric configuration of the electromagnetic field vectors, and "Backward Wave Media" highlights the antiparallel relationship between phase and group velocities. Though these terms are used interchangeably in the literature, "metamaterial" has become the most widely accepted term to denote such materials.

Table 2 divides the material into four fundamental electromagnetic regimes based on the signs of permittivity and permeability. The single-negative cases (ENG and MNG)

produce evanescent waves with imaginary wave vectors, while the double-positive and double-negative cases support propagating waves with real refractive indices of opposite signs.

Table 2: Classification of electromagnetic media by constitutive parameters

Medium type	ϵ_r	μ_r	**Chosen** n	**Wave character**
Double-positive (DPS)	> 0	> 0	$+\sqrt{\epsilon_r \mu_r}$	Propagating, right-handed
Epsilon-negative (ENG)	< 0	> 0	imaginary	Evanescent
Mu-negative (MNG)	> 0	< 0	imaginary	Evanescent
Double-negative (DNG)	< 0	< 0	$-\sqrt{\lvert\epsilon_r\rvert\lvert\mu_r\rvert}$	Propagating, left-handed

2.5 Predicted Electromagnetic Phenomena

Based on this theoretical framework, Veselago mathematically predicted several "reversed" phenomena arising from the antiparallel relationship between $\mathbf{k}$ and $\langle \mathbf{S} \rangle$:

- **Negative Refraction:** At a boundary between media of different handedness, Snell's law still applies, but the refracted ray bends to the *same side* of the interface normal as the incident ray, rather than the opposite side. At an interface which separates right-handed medium 1 ($n_1 > 0$) from left-handed medium 2 ($n_2 < 0$), we have:

$$n_1 \sin\theta_1 = n_2 \sin\theta_2 \quad \text{with } n_2 < 0 \tag{39}$$

  The negative value of n_2 requires θ_2 to be negative which means that the refracted ray emerges on the same side of the normal.

- **Reversed Doppler Effect:** A detector moving toward a radiation source in a left-handed medium observes a frequency shift *downward* (redshift) rather than upward (blueshift), because the phase velocity and group velocity point in opposite directions:

$$\omega_{\text{observed}} = \omega_0 \left(1 - \frac{|n| v}{c}\right) \quad \text{(redshift for approach)} \tag{40}$$

- **Vavilov-Čerenkov Radiation Reversal:** In conventional media, a charged particle moving faster than the phase velocity of light emits radiation in a forward-pointing cone. Veselago predicted that in a left-handed medium, the Čerenkov cone reverses, with radiation emitted in a backward-pointing cone forming an obtuse angle between the particle velocity $\mathbf{v}$ and the energy flux $\langle \mathbf{S} \rangle$.

- **The Veselago Lens (Flat Lens):** It can be shown that a flat slab of left-handed material with $n = -1$ (embedded in air with $n = +1$) could act as a perfect lens which produces a point image of a point object without dispersion or other

distortions. Unlike curved conventional lenses, this flat slab could potentially focus both propagating and evanescent waves, theoretically allowing for imaging beyond the diffraction limit—a concept later elaborated by John Pendry as the "superlens" in 2000 [5].

- **Light Tension:** Unlike the radiation pressure exerted by light on objects in conventional media (pushing force), Veselago predicted that light incident on a reflecting surface in a left-handed medium would impart momentum directed *toward* the source, resulting in a pulling force or "light attraction."

2.6 Engineered Magnetic Response: Pendry (1996, 1999)

John Pendry and collaborators at Imperial College London did the pioneering work for the experimental realization of metamaterials. It was noticed that electromagnetic properties at long wavelengths are determined by the geometric structure of subwavelength elements. He analysed theoertically that by designing periodic arrays of metallic structures much smaller than the operating wavelength, effective permittivity and permeability values can be engineered.

In 1996, Pendry et al. demonstrated that periodic arrays of thin metallic wires could exhibit an effective plasma frequency in the microwave regime, creating materials with negative permittivity at technologically accessible frequencies. Figure 3 gives the scheme of this wire array structure, where metallic rods (with radius r) have been arranged in a periodic lattice with spacing a. When electromagnetic waves with wavelengths much larger than the lattice constant interact with this structure, the collective response of the electron currents in the wires produces an effective negative permittivity, if the frequency of the electromagnetic waves is below a characteristic plasma frequency. This plasma frequency could be tuned by adjusting the wire radius and lattice spacing, pushing the epsilon-negative regime down from optical frequencies (where it occurs naturally in bulk metals) into the microwave range where experimental verification was practical.

The more challenging task was engineering negative magnetic permeability. The nature of the natural magnetic material was determined by their atomic magnetic moments, which become too sluggish to respond at frequencies above a few GHz. Pendry's crucial 1999 breakthrough showed that magnetic responses could be engineered in materials composed entirely of non-magnetic conductors through geometric design. The split-ring resonator (SRR), illustrated in Figure 4, consists of concentric metallic rings with gaps. When it is subjected to an oscillating magnetic field perpendicular to the plane of the rings, currents are induced that create their own magnetic field. Near the resonance frequency of this LC circuit (formed by the inductance of the rings and capacitance of the gaps), the induced magnetic moment can oppose the applied field, yielding an effective negative permeability.

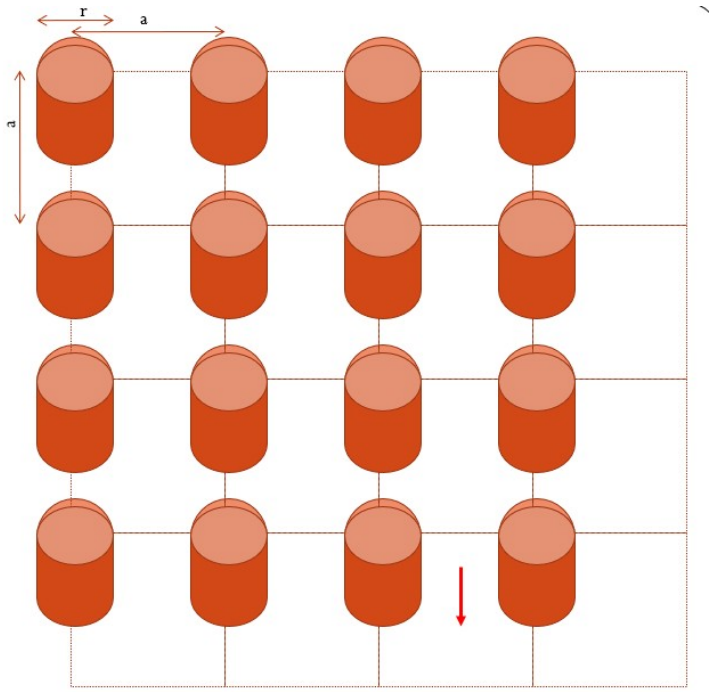

Figure 3: Schematic Periodic array of thin metallic wires for achieving negative effective permittivity. The wires with radius r have been arranged in a square lattice with spacing a. The incident electromagnetic wave direction is indicated by the red arrow. Below the effective plasma frequency, this structure exhibits $\epsilon_{\text{eff}} < 0$.

Pendry's analysis showed that by arranging these SRRs in a periodic array (Figure 4, right panel), one could create a bulk effective medium with tunable magnetic permeability, including negative values over a narrow frequency band. The resonance frequency could be controlled by adjusting the ring dimensions and gap spacing. this allowed the mu-negative regime to be positioned at desired frequencies. Critically, the SRR dimensions must be much smaller than the operating wavelength to satisfy the effective medium approximation.

This work demonstrated that magnetic responses at microwave frequencies could be engineered through subwavelength metallic structures. Combined with the earlier wire array results for negative permittivity, Pendry's work provided the practical blueprint for constructing double-negative metamaterials, transforming Veselago's theoretical predictions into an experimentally testable reality.

2.7 Experimental Demonstration: Smith et al. (2000, 2001)

Pendry's 1996 and 1999 papers provided the essential components—wire arrays for engineered negative permittivity and split-ring resonators for engineered negative permeability—but did not propose combining them to achieve double-negative behavior. The conceptual leap of creating a composite structure exhibiting both negativities simultaneously at the same frequency was made by David Smith and colleagues at the University

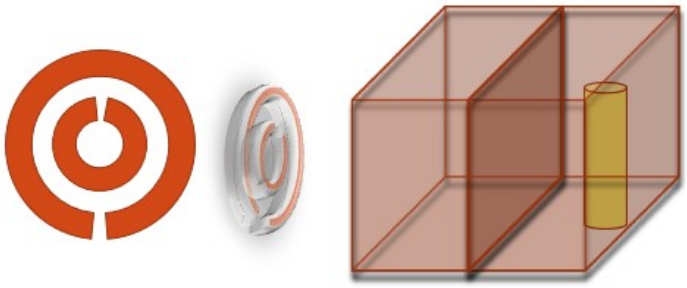

Figure 4: Split-ring resonator (SRR) structure for achieving negative effective permeability. Left: Single SRR unit showing the concentric split rings. Middle: Three-dimensional perspective view of an individual SRR. Right: Periodic array arrangement of SRRs in a cubic lattice. Near the resonance frequency, this structure exhibits $\mu_{\text{eff}} < 0$.

of California, San Diego.

Smith et al. in his landmark 2000 paper, proposed and experimentally demonstrated the first artificial metamaterial with simultaneously negative permittivity and permeability. They acknowledged that Pendry's two separate inventions could be integrated into a single periodic structure. By combining wire arrays (providing $\epsilon_{\text{eff}} < 0$ below their plasma frequency) with interspaced split-ring resonators (providing $\mu_{\text{eff}} < 0$ near their magnetic resonance), they created a composite medium with a frequency window where both constitutive parameters were simultaneously negative.

The critical engineering challenge was ensuring spectral overlap between the two negative regimes. The wire array produces negative permittivity below its effective plasma frequency ω_p, while the SRR structure exhibits negative permeability in a narrow band near its resonance frequency ω_0. Through careful design of the geometric parameters—wire spacing and diameter, SRR dimensions, gap size, and the relative positioning of wires and rings within the unit cell—Smith et al. achieved a frequency window from approximately 4.5 to 5.0 GHz where both $\epsilon_{\text{eff}} < 0$ and $\mu_{\text{eff}} < 0$ simultaneously.

The experimental verification employed microwave transmission measurements through a two-dimensional array of the composite structure. When SRRs alone were tested with magnetic field polarized parallel to the ring axes, a stopband appeared from 4.2 to 4.6 GHz due to negative permeability. When metal wires alone were tested, they produced a stopband extending from zero frequency up to their plasma frequency at 12 GHz due to negative permittivity. Remarkably, when both elements were combined in the composite structure, a passband appeared within the previously forbidden frequency range—precisely where both ϵ and μ were negative. This dramatic transformation from stopband to passband when combining two individually attenuating structures provided compelling evidence that the composite medium was indeed supporting electromagnetic propagation in the double-negative regime.

Smith et al. derived an approximate dispersion relation for the composite structure by combining the plasma-like behavior of the wire medium with the resonant permeability of the SRR array:

$$k^2 = \frac{\omega^2 - \omega_p^2}{c^2} \cdot \frac{\omega^2 - \omega_b^2}{\omega^2 - \omega_0^2} \tag{41}$$

where ω_0 is the magnetic resonance frequency of the SRRs, ω_p is the effective plasma frequency of the wire array, and $\omega_b = \omega_0\sqrt{1-F}$ with F being the fractional area of the unit cell occupied by the interior of the split rings. This expression reveals that the passband extends from ω_0 to ω_b, with a bandwidth independent of the plasma frequency (provided $\omega_p > \omega_b$). Critically, this dispersion relation exhibits negative group velocity everywhere within the passband—the defining signature of a left-handed medium where phase velocity and energy flow are antiparallel.

The following year, Smith, Shelby, and Schultz demonstrated negative refraction at the interface between the metamaterial and air, directly confirming Veselago's 1964 prediction that electromagnetic waves would refract to the "wrong side" of the interface normal in double-negative media. This experimental observation of negative refraction provided unambiguous proof that the composite structure was not merely supporting some exotic guided mode, but was genuinely functioning as a bulk medium with negative refractive index. Thirty-six years after Veselago's theoretical prediction, his revolutionary physics could finally be tested in the laboratory.

The Smith demonstration transformed metamaterials from a theoretical curiosity into an experimental reality, opening an entirely new field of electromagnetic engineering and validating Veselago's prescient 1964 analysis.

3 Physical Mechanisms

In order to understand how metamaterials achieve negative electromagnetic parameters, one must first examine the microscopic origins of permittivity and permeability in conventional materials.

3.0.1 Electric Permittivity

The relative permittivity ϵ_r quantifies how readily a material develops electric polarization $\mathbf{P}$ in response to an applied electric field $\mathbf{E}$. At the microscopic level, the electric field induces displacement of charge distributions in atoms or molecules, creating electric dipole moments. The constitutive relation is:

$$\mathbf{D} = \epsilon_0\mathbf{E} + \mathbf{P} = \epsilon_0\epsilon_r\mathbf{E} \tag{42}$$

In oscillating electromagnetic fields, the induced polarization responds as a driven

harmonic oscillator. Near electronic resonances, the polarization lag behind the driving field by nearly 180°, thereby resulting in negative permittivity. This occurs naturally in metals at frequencies below the plasma frequency.

3.0.2 Magnetic Permeability

The relative permeability μ_r quantifies the material's magnetic response, characterized by magnetization $\mathbf{M}$ in response to a magnetic field $\mathbf{H}$:

$$\mathbf{B} = \mu_0(\mathbf{H} + \mathbf{M}) = \mu_0\mu_r\mathbf{H} \tag{43}$$

Natural magnetic responses arise from orbital motion of electrons and unpaired electron spins.

3.1 Achieving Negative Permittivity: Metallic Wire Arrays

Natural metals exhibit negative permittivity below their plasma frequency ω_p. Pendry et al. demonstrated that arrays of thin metallic wires can mimic metals with dramatically reduced plasma frequencies, bringing negative permittivity into the microwave regime [7].

The effective plasma frequency of a wire array is:

$$\omega_{p,\text{eff}}^2 = \frac{2\pi c^2}{a^2 \ln(a/r)} \tag{44}$$

where a is the lattice spacing and r is the wire radius. The permittivity is then:

$$\epsilon_{\text{eff}}(\omega) = 1 - \frac{\omega_{p,\text{eff}}^2}{\omega^2} \tag{45}$$

For $\omega < \omega_{p,\text{eff}}$, the effective permittivity becomes negative. The reduction in plasma frequency compared to bulk metals occurs because: (1) the effective density of conduction electrons is reduced in the wire array, and (2) the effective electron mass increases when electrons are confined to thin wires. This "diluted metal" approach enables engineering negative permittivity with small losses at microwave and lower frequencies.

3.2 Achieving Negative Permeability: Split-Ring Resonators

The most significant breakthrough enabling practical metamaterials was Pendry et al.'s demonstration that split-ring resonators (SRRs) can produce strong magnetic responses at microwave and higher frequencies [8].

An SRR consists of concentric metallic rings with gaps. When it is subjected to an oscillating magnetic field perpendicular to the ring plane, currents are induced that create magnetic dipole moments. It is noteworthy that:

- The gap prevents currents from freely circulating, dramatically increasing the resonance frequency compared to solid rings
- The gap acts as a capacitor while the rings act as an inductor, forming an LC resonant circuit
- At the resonance frequency $\omega_0 = 1/\sqrt{LC}$, the magnetic response is maximized
- Just below resonance, the induced magnetic dipole lags the applied field by approximately 180°, producing negative permeability

The effective permeability of an SRR medium is:

$$\mu_{\text{eff}}(\omega) = 1 + \frac{F\omega^2}{\omega_0^2 - \omega^2 - i\Gamma\omega} \tag{46}$$

where F is the geometric filling factor and Γ represents losses. For ω slightly below ω_0, μ_{eff} becomes negative.

The resonance frequency can be tunedby adjusting the SRR geometry, allowing negative magnetic response across a wide range of frequencies. This tunability is crucial for practical metamaterial applications.

4 Exotic Electromagnetic Phenomena

Veselago's 1964 theoretical analysis predicted that double-negative media would exhibit a suite of electromagnetic phenomena fundamentally different from those observed in conventional materials. When both permittivity and permeability are simultaneously negative, the left-handed arrangement of field vectors $(\mathbf{E}, \mathbf{H}, \mathbf{k})$ reverses familiar electromagnetic behaviors. The principal exotic electromagnetic phenomena in negative-index metamaterials include:

1. **Negative Refraction and Reversed Snell's Law:** Electromagnetic waves refract to the same side of the interface normal as the incident wave, enabling flat lenses and novel beam steering devices.
2. **Perfect Lens and Subwavelength Imaging:** A slab with $n = -1$ can focus both propagating and evanescent waves, overcoming the diffraction limit and achieving resolution beyond $\lambda/2$.
3. **Electromagnetic Cloaking and Invisibility:** Transformation optics combined with certain kind of metamaterials enables the design of cloaking devices that guide electromagnetic waves smoothly around concealed objects and the objects are not usually identified.

4. **Reversed Doppler Effect:** A source moving toward an observer is expected to produce a frequency decrease rather than increase, which is the case of the familiar Doppler shift.

5. **Reversed Cherenkov Radiation:** when a charged particle moves faster than the phase velocity in a DNG medium, it emits radiation in the backward direction, opposite to their motion.

We examine each of these phenomena in detail, explaining the underlying physics and discussing experimental demonstrations where available.

4.1 Negative Refraction and Reversed Snell's Law

The most fundamental consequence of negative refractive index is negative refraction. It is schematically illustrated in Figure 5. It is observed that at the interface between a positive-index medium (air) and a negative-index medium (NIM), the behavior of light is opposite to that in conventional refraction in DPS-DPS interface.

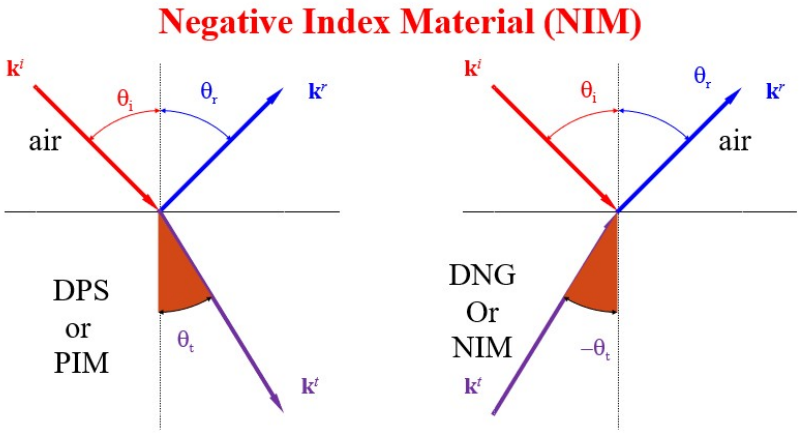

Figure 5: Comparison of refraction at interfaces. Left: Conventional refraction at an air-DPS (double-positive/positive-index material) interface. The transmitted ray $\mathbf{k}^t$ bends to the opposite side of the interface normal from the incident ray $\mathbf{k}^i$, with transmission angle θ_t. Right: Negative refraction at an air-DNG (double-negative/negative-index material) interface. The transmitted ray bends to the *same* side of the normal as the incident ray, with angle $-\theta_t$, demonstrating reversed Snell's law. In both cases, $\mathbf{k}^r$ represents the reflected ray at angle $\theta_r = \theta_i$.

On the left of the figure 5 , light incident from air onto a double-positive (DPS) or positive-index material (PIM) refracts in the familiar way: the incident ray $\mathbf{k}^i$ at angle θ_i produces a transmitted ray $\mathbf{k}^t$ at angle θ_t on the *opposite* side of the interface normal. The reflected ray $\mathbf{k}^r$ follows the standard law of reflection which requires $\theta_r = \theta_i$. On the right of the figure 5, a similar incident ray encounters a double-negative (DNG) or negative-index material (NIM). The transmitted ray now appears on the *same* side of the

interface normal as the incident ray, with refraction angle labeled as $-\theta_t$ to emphasize this reversal.

Mathematically, Snell's law at the air-NIM interface takes the form:

$$n_{\text{air}} \sin\theta_i = |n_{\text{NIM}}| \sin\theta_t \tag{47}$$

where $n_{\text{NIM}} < 0$. Though the magnitudes of the angles have the same relationship as in conventional refraction, but the geometric configuration is reversed. This reversal occurs because the wave vector $\mathbf{k}$ is antiparallel to the Poynting vector $\mathbf{S}$ in the NIM.As we know that the vector $\mathbf{k}$ determines the phase front direction and the vector $\mathbf{S}$ determines the direction of energy flow. While the phase fronts propagate toward the interface normal, the electromagnetic energy flows away from it. The first experimental demonstration of negative refraction by Shelby, Smith, and Schultz in 2001 [4] provided direct confirmation of Veselago's 1964 prediction and validated the reality of negative-index metamaterials.

4.2 Perfect Lens and Subwavelength Imaging

Pendry's perfect lens concept [5] represents one of metamaterials' most revolutionary applications. A slab of material with $n = -1$ (equivalently $\epsilon = \mu = -1$) placed between an object and image plane can achieve perfect focusing beyond the diffraction limit, as illustrated in Figure 6.

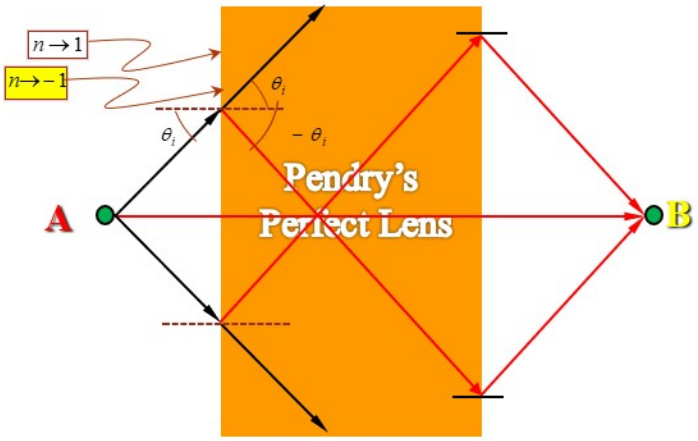

Figure 6: Pendry's perfect lens: A slab with refractive index $n = -1$ focuses light from point source A to image point B. The negative refractive index causes rays to refract to the same side of the interface normal (angles θ_i and θ_t shown), creating two focal points—one inside the slab and one at the image plane B. The black rays represent propagating wave components.

Figure 6 shows how light from a point source A is perfectly focused to point B through the negative-index slab. The rays refract anomalously at both interfaces: unlike conventional refraction where light bends to opposite sides of the normal, here the transmitted

rays lie on the *same* side of the interface normal as the incident rays. This negative refraction creates an unusual focusing behavior—the rays converge to an intermediate focus inside the slab, then diverge, and finally converge again at the image point B outside the slab. This double-focusing geometry is unique to negative-index materials.

Conventional lenses are limited by diffraction to resolution $\sim \lambda/2$ because they cannot focus evanescent waves—field components with imaginary wave vectors that decay exponentially from the source. These evanescent waves carry fine spatial details but are lost in conventional imaging.

A perfect lens operates through two complementary mechanisms:

1. **Propagating waves:** Negative refraction at both interfaces (visible in Figure 6 as the black ray paths) focuses propagating wave components to geometric points inside and beyond the slab, reconstructing the far-field image.

2. **Evanescent waves:** The negative permittivity and permeability cause evanescent components to *grow* exponentially rather than decay while traversing the slab. This exactly compensates for their natural decay outside the slab., and thus restores the complete evanescent spectrum at the image plane, reconstructing subwavelength details.

By preserving both propagating and evanescent components, the perfect lens reconstructs the complete near-field of the object at point B, achieving resolution limited only by material losses and fabrication precision rather than wavelength. While theoretically exact for the idealized case ($\epsilon = \mu = -1$), practical perfect lenses face significant challenges from material losses, impedance matching difficulties, narrow bandwidth, and fabrication precision requirements.

4.3 Electromagnetic Cloaking and Invisibility

Enginnering community working in the field of transformation optics is exploring the properties of metamaterials to design electromagnetic cloaking devices that make the objects invisible to electromagnetic radiation. The basic concept is simple and can be explained through a simple example. Let us take example of a metallic cylinder as an object, that blocks light coming from one direction, and thus casts a shadow and reflects light backward. Ordinarily, both the shadow and reflected light reveal the cylinder's presence. If this the cylinder is covered with a carefully designed cylindrical shell of cloaking material, the light can be guided smoothly around the hidden object. If the cloaking shell is engineered to have precise gradient of dielectric properties, it bends incoming light rays around the concealed cylinder and then returns them to their original paths, as if the object were not present. For an external observer, no shadow appears and minimal reflection occurs, leaving almost no trace of the concealed object.

Practical optical cloaking devices face several challenges. The impedance mismatch between the cloak and free space produces approximately 4% power reflection. Material losses in the metal-dielectric composite, though small (imaginary part of permittivity $\sim$0.1), weaken the cloaking effect. The design operates only over a narrow frequency range because the curved light trajectory requires an effective refractive index less than unity, which by causality must be dispersive. Fabrication requires precise control over nanowire dimensions and spacing across the entire cloaking shell. Nevertheless, finite-element simulations demonstrate that even with these imperfections, such cloaks dramatically reduce scattering compared to the uncloaked case, with wave fronts flowing smoothly around the cloaked region and minimal shadow formation.

Beyond optical frequencies, electromagnetic cloaking has been successfully demonstrated at microwave frequencies. While perfect invisibility remains beyond current capabilities, these devices represent a remarkable validation of transformation optics principles and demonstrate the power of metamaterial engineering to manipulate electromagnetic wave propagation in unprecedented ways.

4.4 Reversed Doppler Effect

Veselago predicted that in negative-index materials, the Doppler effect would be reversed. In conventional media, an observer approaching a source experiences a blue shift: $f_{\text{observed}} = f_0(1 + nv/c)$. In DNG media where phase velocity and group velocity are antiparallel, the same motion produces a red shift: $f_{\text{observed}} = f_0(1 - |n|v/c)$. While analyzed theoretically and demonstrated in transmission line metamaterial analogues, experimental verification in electromagnetic metamaterials at microwave or optical frequencies remains challenging.

4.5 Reversed Cherenkov Radiation

Cherenkov radiation occurs when a charged particle moves through a medium with a velocity greater than the phase velocity of light in that medium. In conventional materials, the radiation forms a cone with the particle at the apex, with radiation emitted at an angle θ given by:

$$\cos\theta = \frac{c}{nv} \tag{48}$$

where v is the particle velocity. The radiation propagates away from the particle trajectory.

In negative-index metamaterials, the radiation cone is reversed. The phase velocity and group velocity are antiparallel, so while the wave fronts still form the characteristic cone, the energy propagates *backward* toward the particle rather than away from it [10].

The angle becomes obtuse:

$$\cos\theta = \frac{c}{|n|v} \quad \text{with} \quad \theta > 90 \tag{49}$$

This reversal has been experimentally demonstrated and may enable novel particle detectors and radiation sources with unprecedented directional control.

5 Metamaterials for Energy Applications

Beyond their fundamental scientific interest, metamaterials have shown promise for several energy-related applications.A few of these are briefly discussed below.

5.1 RF Energy Harvesting

Metamaterial-based designs can enhance radiofrequency energy harvesting efficiency. In 2013, Hawkes and colleagues at Duke University demonstrated a microwave metamaterial with integrated power harvesting, achieving 36.8% rectification efficiency for a 900 MHz signal [13]. The structure consisted of split-ring resonators coupled to rectifying diodes. The key advantage is resonant field enhancement at subwavelength dimensions, enabling compact antennas for potentially harvesting ambient Wi-Fi or cellular signals, though low ambient power density presents practical challenges.

5.2 Wireless Power Transmission

Metamaterials can enhance wireless power transfer through improved magnetic coupling. Wu and colleagues demonstrated in 2013 that a metamaterial slab with negative permeability between magnetically coupled resonators significantly enhances coupling [14]. Using a perfect magnetic conductor reflector in simulations, they increased efficiency from 48% to 72%. The mechanism is magnetic flux channeling: negative permeability concentrates field lines between coils, enabling efficient transfer over larger distances with greater tolerance to misalignment.

5.3 Enhanced Solar Energy Conversion

Atwater and Polman analyzed how metamaterial structures could enhance solar cell performance [**?**]. Metamaterials with engineered refractive index profiles can provide broadband antireflection coatings covering the visible and near-infrared spectrum, with wide-angle response reducing sensitivity to sun position. However, practical implementation requires balancing optical performance against material costs and manufacturing complexity.

5.4 Thermophotovoltaic Energy Conversion

Thermophotovoltaic systems convert thermal radiation into electricity using photovoltaic cells. Unlike solar cells accepting the fixed solar spectrum, TPV systems can engineer both emitter and receiver for optimal spectral matching. In 2016, Kruk and colleagues demonstrated a metamaterial thermal emitter exhibiting magnetic hyperbolic dispersion [12]. The metamaterial—alternating nanoscale layers of gold and magnesium fluoride—radiates preferentially in specific spectral bands and directions rather than thermally in all directions. This directional, spectrally selective emission can be matched to thermophotovoltaic cell bandgaps, potentially improving efficiency. Thermophotovoltaic systems offer continuous operation independent of sunlight, using stored thermal energy or combustion sources, though practical systems face challenges from material losses and manufacturing complexity.

6 Future Directions and Challenges

The metamaterial field continues to expand, though significant challenges remain before accessible practical applications can be realized.

Optical-frequency metamaterials require nanoscale feature control over a large macroscopic areas. This can be achieved only through expensive techniques like electron-beam lithography. Material losses increase sharply with frequency, severely limiting performance at optical wavelengths. Large scale manufacturing may have its own problems

Several promising extensions of metamaterial concepts are being actively investigated. Nonlinear metamaterials were designed by incorporating varactors or optical Kerr media. These enabled tunable and reconfigurable electromagnetic responses. Active metamaterials were integrated with semiconductor devices or MEMS structures to have dynamic control of properties. The metamaterial framework has been successfully extended to acoustic and elastic waves. This has enabled exotic phenomena like sound cloaking and vibration isolation.

7 Conclusions

Metamaterials are an interesting example when theoretical investigations preceded experimental realisation of the concepts. It took 33 years from Veselago's theoretical predictions in 1968 to experimental demonstrations in the 2000s. Since then, metamaterials have evolved from theoretical curiosities to practical devices addressing real-world challenges. The exotic phenomena exhibited by metamaterials are of sincere interest of the researchers and inspire new applications. In the energy sector, metamaterials show particular promise for harvesting ambient RF radiation to power distributed sensor networks,

enabling efficient wireless power transmission across various distance scales, enhancing solar cell light collection and absorption, improving thermophotovoltaic conversion efficiency through spectral selectivity. While challenges remain in fabrication, integration, and scaling to commercial production, the rapid progress in metamaterial science and technology suggests that these revolutionary materials will play an increasingly important role in technology including future energy systems.

References

[1] V.G. Veselago, "The electrodynamics of substances with simultaneously negative values of ϵ and μ," *Soviet Physics Uspekhi*, vol. 10, no. 4, pp. 509–514, 1968.

[2] J.H.E. Griffiths, "Anomalous High-frequency Resistance of Ferromagnetic Metals," *Nature*, vol. 158, no. 4019, pp. 670–671, 1946.

[3] D.R. Smith, W.J. Padilla, D.C. Vier, S.C. Nemat-Nasser, and S. Schultz, "Composite medium with simultaneously negative permeability and permittivity," *Physical Review Letters*, vol. 84, no. 18, pp. 4184–4187, 2000.

[4] R.A. Shelby, D.R. Smith, and S. Schultz, "Experimental verification of a negative index of refraction," *Science*, vol. 292, no. 5514, pp. 77–79, 2001.

[5] J.B. Pendry, "Negative refraction makes a perfect lens," *Physical Review Letters*, vol. 85, no. 18, pp. 3966–3969, 2000.

[6] C. Kittel, *Introduction to Solid State Physics*, 8th ed. Hoboken, NJ: Wiley, 2005.

[7] J.B. Pendry, A.J. Holden, D.J. Robbins, and W.J. Stewart, "Extremely low frequency plasmons in metallic mesostructures," *Physical Review Letters*, vol. 76, no. 25, pp. 4773–4776, 1996.

[8] J.B. Pendry, A.J. Holden, D.J. Robbins, and W.J. Stewart, "Magnetism from conductors and enhanced nonlinear phenomena," *IEEE Transactions on Microwave Theory and Techniques*, vol. 47, no. 11, pp. 2075–2084, 1999.

[9] W. Cai, U.K. Chettiar, A.V. Kildishev, and V.M. Shalaev, "Optical cloaking with metamaterials," *Nature Photonics*, vol. 1, no. 4, pp. 224–227, 2007.

[10] S. Xi, H. Chen, T. Jiang, L. Ran, J. Huangfu, B.-I. Wu, J.A. Kong, and M. Chen, "Experimental verification of reversed Cherenkov radiation in left-handed metamaterial," *Physical Review Letters*, vol. 103, no. 19, p. 194801, 2009.

[11] H.A. Atwater and A. Polman, "Plasmonics for improved photovoltaic devices," *Nature Materials*, vol. 9, no. 3, pp. 205–213, 2010.

[12] S. Kruk, Z.J. Wong, E. Pshenay-Severin, K. O'Brien, D.N. Neshev, Y.S. Kivshar, and X. Zhang, "Magnetic hyperbolic optical metamaterials," *Nature Communications*, vol. 7, p. 11329, 2016.

[13] A.M. Hawkes, A.R. Katko, and S.A. Cummer, "A microwave metamaterial for energy harvesting," *Applied Physics Letters*, vol. 103, no. 16, p. 163901, 2013.

[14] J. Wu, B. Wang, W.S. Yerazunis, and K.H. Teo, "Wireless Power Transfer with Artificial Magnetic Conductors," *Technical Report TR2013-018*, Mitsubishi Electric Research Laboratories, 2013.